Aerodynamic characteristics of wind turbine blade airfoils at high angles-of-attack

W.A. Timmer
Delft University of Technology
Faculty of Aerospace Engineering
Kluyverweg 1, 2629 HS Delft, The Netherlands
w.a.timmer@tudelft.nl

Abstract

Airfoil characteristics at deep stall angles were investigated. It appeared that the maximum drag coefficient as a function of the airfoil upwind y/c ordinate at x/c=0.0125 can be approximated by a straight line. The lift-drag ratios in deep stall of a number of airfoils with moderate lower surface thickness coincide. It was found that the lift-drag ratio of airfoils with leading edge separation is independent of aspect ratio. The lift-drag ratios of the various sections of a non-rotating and a rotating blade in deep stall coincide with the two-dimensional curve.

Keywords: Airfoil characteristics, lift-to-drag ratio, high angles of attack.

1 Introduction

During standstill, starts and stops, the blade of a wind turbine is subjected to large angles-of-attack. In these situations the blade acts as a medium aspect ratio wing. To calculate the blade loads, the characteristics of blade segments are in general related to the two-dimensional aerodynamic characteristics of the airfoils measured in the wind tunnel. There is quite some uncertainty how to translate the 2D characteristics to the non-rotating blade loads, but even large discrepancies exist in the data of two-dimensional wind tunnel tests on airfoils at high angles of attack. This is often the result of differences in test setup, in the measurement of the test section dynamic pressure (due to blockage effects) and in the applied wind tunnel wall correction scheme. To be able to address these uncertainties and to further map the DU airfoils performance at Delft University of Technology a number of wind turbine airfoils have been tested at high angles of attack for Reynolds numbers up to $Re=0.7x10^6$ and results of tests found in literature have been studied. A second goal was to investigate if some general description of airfoil key parameters would be possible on the basis of the existing data at high angles of attack.

2 Lift and drag data from various sources

2.1 Measurements on NACA 0012

Fig. 1 shows measurements on airfoil NACA 0012 from various sources [1,2,3,4,5] in the Reynolds number range from 500,000 to approximately 750,000. The figure shows that in fact the only agreement between the curves is the value of the lift coefficient at 0, 23 and 90 degrees angle of attack. All other values differ. The same mismatch can be found in the drag data. It appears that testing the same airfoil at high angles of attack not a priori renders comparable results.

2.2 Non-symmetrical airfoils

In literature a number of studies can be found dealing with wind tunnel measurement of non-symmetrical airfoils at high angles of attack. Most referenced are the tests on NACA 63_2-215 [6] and LS(1)-0417 [7] and those on the NACA 44 series [8]. For these airfoils the lift and drag at high angles of attack is depicted in figures 2a and b.

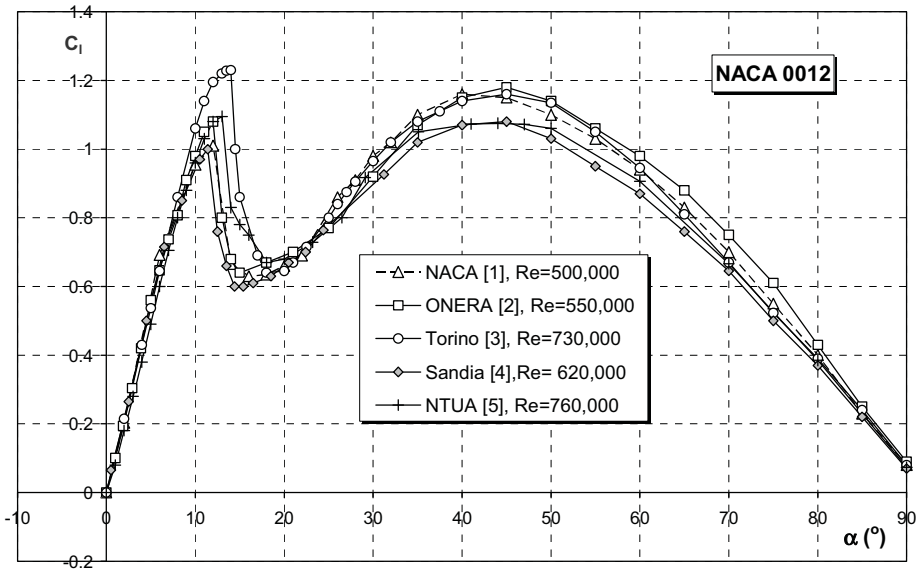

Figure 1: Measured two-dimensional aerodynamic characteristics of airfoil NACA 0012

The data for the NACA 4418 airfoil are at a much lower Reynolds number compared to the other two, since the data in [8] for the higher Reynolds numbers did not go beyond 60 degrees. It appeared, however, that there was no distinct difference between the low and the higher Reynolds numbers at high incidences. The tests on the 18% thick DU-96-W-180 and the 30% thick DU 97-W-300 were already published in [9]. Figure 3 shows the airfoil performance of both airfoils at a Reynolds number of 0.7×10^6. To the data in the low drag region the classical wind tunnel wall corrections for solid and wake blockage and streamline curvature have been applied. In case of leading edge separation an alternative bluff body correction has been used, following the guidelines of Hackett and Cooper [10].

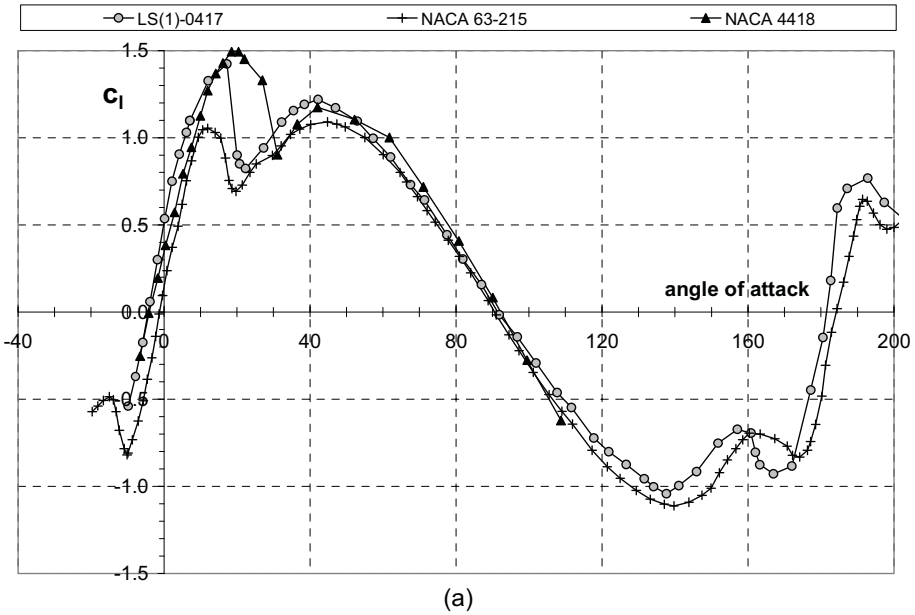

(a)

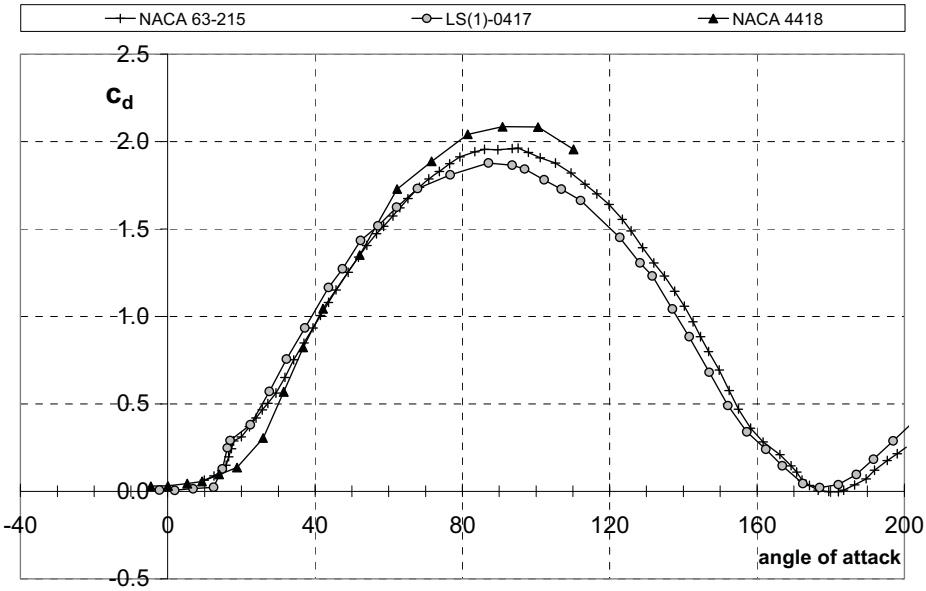

(b)

Figure 2: The lift (a) and drag (b) curves for three airfoils at high angles of attack. LS(1)-0417: Re=0.67x10^6, NACA 63-215: Re= 0.55x10^6, NACA 4418: Re= 0.25x10^6

3 The maximum drag coefficient

Apart from other distinct differences associated with the airfoil maximum thickness and the trailing edge thickness figure 3 shows a noticeable difference in the maximum drag coefficient of the airfoils at 90 degrees and a very small one at 270 degrees. However, figure 2b shows larger differences between airfoils with moderate thickness. Since all airfoils have one relatively sharp edge when they are placed normal to the flow, differences in maximum drag are strongly related to the contour of the leading edge coefficient.

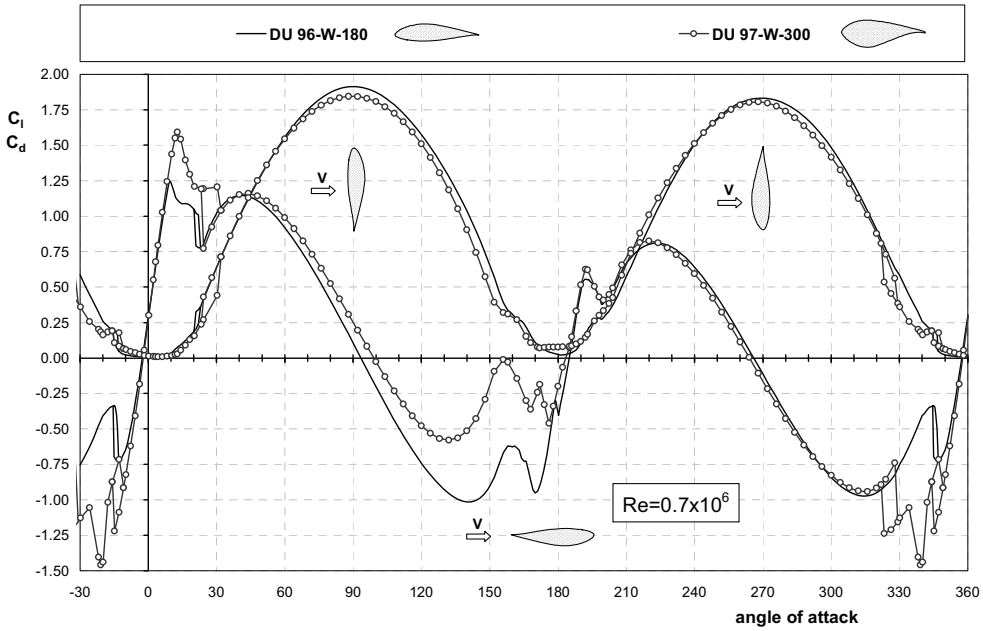

Figure 3: The performance of 2 DU airfoils at angles-of-attack ranging from 0 to 360 degrees

More in particular the thickness of the upwind side close to the airfoil leading edge is of interest here. In [11] Lindenburg correlates the maximum value of C_d to the leading edge radius and the flow direction at the trailing edge, also on the basis of several other shapes found in literature such as wedges and (half-)cylinders. A simpler approach is followed here to find a relation between the maximum value of C_d and the airfoil contour.
In table 1 the maximum drag coefficient is related to the upwind thickness of the airfoil leading edge, taken as the y/c ordinate at x/c=0.0125. The table is graphically represented in figure 4. Though the choice of this chord location is rather arbitrary (and also the contour gradient at some leading edge location may work), here the study of Gault [12] is followed, who correlated the stalling characteristics of a large number of low-speed airfoil sections with this ordinate.

Table 1: The maximum C_d as a function of the upwind thickness of the leading edge

Airfoil	y/c at x/c=0.0125	$C_{d\text{-}max}$	Ref.
Flat plate	0	1.980	[13]
NACA 63-215	0.01793	1.960	[7]
LS(1)-0417, 90 degr.	0.02129	1.877	[6]
LS(1)-0417, 270 degr.	0.03011	1.800	
DU 96-W-180, 90 degr.	0.01533	1.914	[9]
DU 96-W-180, 270 degr.	0.02072	1.832	
NACA 0012	0.01894	1.914	[5]
NACA 0018	0.02841	1.800	[14]
DU 91-W2-250	0.03100	1.859	[14]
DU 97-W-300, 270 degr.	0.03069	1.806	[9]
DU 97-W-300, 90 degr.	0.03327	1.845	

This approach also worked quite well for the angle of deep stall onset derived in [9]. The upwind contour of the airfoil is important. As long as the downwind side of the object does not project deep into the wake it has virtually no effect on the resulting drag coefficient. When the relation is approximated by a straight line the function reads:

$$C_{d,max}=1.994-5.4375*y/c \qquad (1)$$

The predictive value of equation (1) is ± 3%, which is within the assumed experimental error in the various studies.
It is interesting to note that a comparable solution can be found when two extremities between walls are considered: a flat plate with two sharp edges normal to the flow with a C_d of 1.98 [13] having a y/c=0 and a half-cylinder with the round side pointing upwind with a drag coefficient of 1.16 [13], having a y/c ordinate at the x/c=0.0125 location of 0.1576. If we assume the maximum drag

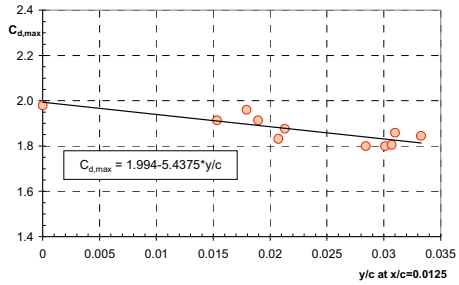

Figure 4: The relation between airfoil leading edge thickness and the $C_{d,max}$

coefficient of all the airfoils lying on the straight line between these two points, the airfoils are related by

$$C_{d,max}=1.980-5.203*y/c \qquad (2)$$

The value of the maximum drag coefficient at 90 degrees for the DU 96-W-180 airfoil (y/c=0.01533) using equation (2) is 1.90, which is less than 1 % off the measured value given in table 1. However, strictly speaking the half-cylinder's C_d is too low to be in table 1, since it has one rounded upwind edge more than the airfoils. In equation (1) also recent wind turbine airfoils are included with a thickness ranging from 0 to 30% and it seems unlikely that other dedicated wind turbine airfoils falling into this range will have a maximum drag coefficient departing appreciably from this relation.

4 The relation between lift and drag at high angles.

According to equation (1) the maximum value of the drag coefficient will not exceed 2.0. However, as is also shown in figure 2b, in literature (e.g. ref [3]) a number of test campaigns report values well over 2.0. This may be the consequence of an erroneous recording of the forces or the test section dynamic pressure (including correcting thereof for wind tunnel wall effects), or an insufficiently long time averaging, since the flow is highly unsteady at these angles. An error in the dynamic pressure of 4 to 5% may easily lead to values above 2. In general the measurements are performed with a balance system and the

coefficients result from dividing the forces by q*S, S being the model area. With a dynamic pressure error the coefficients from these tests may give a deviant picture of the characteristics in separate lift and drag graphs, but the value of the lift-to-drag ratio does not show this error. Since most test data have been corrected with the classical method of Maskell, in [10] labelled as the first step in the two-step method of Hackett, the data have been corrected for wake blockage only and the corrections are applied as a dynamic pressure change. Taking the lift-drag ratio this correction and also a possible error in the dynamic pressure will cancel out.

4.1 Origin of lift and drag at deep stall angles

The origin of both the lift and the drag forces lies in the pressure distribution of the airfoil, which is severely dominated by the separated region of the upper surface. As was already mentioned before in this paper the upper surface thickness of the airfoil can be neglected when the airfoil is positioned normal to the flow. In fact, with leading edge separation present on the upper surface this must also be true for angles in the entire deep stall region. The normal force is very strongly related to the upper surface average pressure level, which in its turn is directly related to the angle of attack. The lower surface is completely laminar, and its contribution to the overall drag force is very small. This may lead to the assumption that for airfoils with moderate thickness of the lower surface and camber the lift-drag ratio's may be the same. In figure 5 the lift-drag ratio's for 3 airfoils with a thickness ranging from 12% to 18% is shown as a function of the deep stall angle.

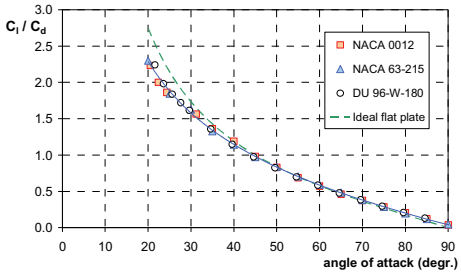

Figure 5: The lift drag ratio of three airfoils with varying thickness at high angles of attack compared to ideal flat plate theory.

As can be concluded from the graph the lift-drag ratio for the three airfoils compare quite well, but differ from the value shown by ideal flat plate theory as given in:

$$C_l = 2 * \sin\alpha * \cos\alpha \quad (3)$$

$$C_d = 2 * \sin^2\alpha \quad (4)$$

In the angle of attack range from 30 to 80 degrees the airfoil curves coincide. The solid line is the trend line of NACA 63-215.

4.2 The effect of aspect ratio

If the lift-drag ratios for different airfoils coincide this may also hold for the lift-drag ratio of the same airfoil but with different aspect ratio. Induced effects of aspect ratio will obviously change the flow field but, since the entire upper surface flow is dominated by a separated flow region, the

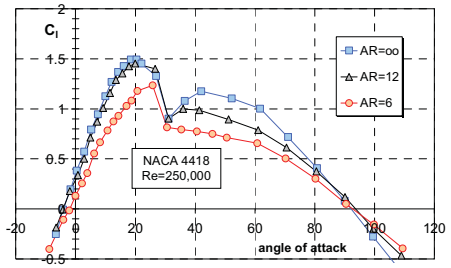

(a)

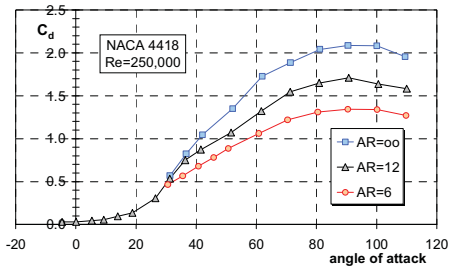

(b)

Figure 6: The lift (a) and drag (b) data of airfoil NACA 4418 [8] for various aspect ratios.

resulting ratio of the forces may very well be of the same order as in the two-dimensional case.
In figure 6 the lift and drag curves of airfoil NACA 4418 [8] for various aspect ratios are shown. The lift curve for aspect ratio 6 lies well below the two-dimensional configuration and the drag for AR=6 is

more than 35% lower compared to the infinite aspect ratio.

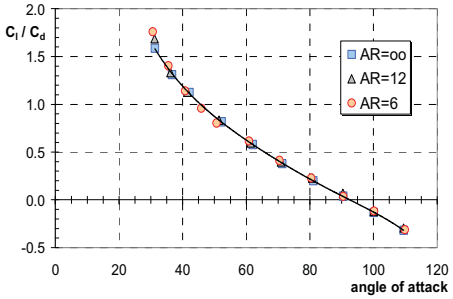

Figure 7: The lift-drag ratios for three aspect ratios of airfoil NACA 4418 [8]

Figure 7 demonstrates the lift-drag ratio of the configurations depicted in figure 6. The graph shows that the lift-drag ratio for aspect ratios 12 and 6 coincides with the curve for two-dimensional flow.

5 Blade forces on a non-rotating blade.

Since figure 7 confirms that the lift-drag ratio's of the two-dimensional configuration and the various aspect ratio's give the same result, the assumption can be made that the same relation holds for the two-dimensional value of an airfoil and the non-rotating blade.
In figure 8 the lift and drag coefficients at three blade stations are shown for the NREL UAE phase VI blade measured in the NASA Ames wind tunnel at Langley, USA. The curves are taken from [15], where the measured pressure distributions were coupled to the right angle of attack by corrections on the local inflow angle measured with a 5-hole probe. These corrections include angle of attack changes due to the upflow in front of the airfoil calculated by the Biot and Savart law and smaller corrections due to a 0.9 degree blade pitch misalignment, a 5-hole probe misalignment and the difference in twist between the location of the probe and the nearest blade station at which the pressure distributions were measured. By iteration the lift and drag coefficients were calculated from the estimated angle of attack and the airfoil normal and tangential force coefficients from the pressure distributions. Not all data points for the non-rotating blade are shown here. For the higher angles averaged data points were presented in [15] and they were also used in the graphs of figure 8. Also in the figure the two-dimensional characteristics as measured in the CSU-wind tunnel [15].
The CSU wind tunnel data show a two-dimensional C_d at 90 degrees well over 2. On the basis of figure 4 a $C_{d,max}$ of 1.913 would be expected (y/c=0.01504).

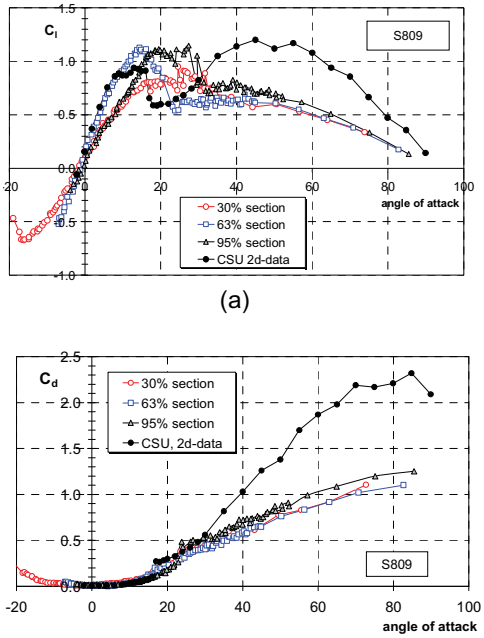

Figure 8: The lift (a) and drag (b) curves for the non-rotating blade [15] and the two-dimensional characteristics at a Reynolds number of 500,000 from the CSU wind tunnel.

Since the blade in the non-rotating configuration is a wing of finite length the resulting lift and drag force coefficients show much lower values in the deep stalled region compared to the 2d case. End effects seem to be more visible in the 30% section data than at the 95% station. The maximum lift at the 63% and 95% sections is much higher than in the 2d case. This is believed to be caused for the greater part by the difference in Reynolds number. The non-rotating blade measurements were made at an average wind velocity of 30.2 m/s. This results in the Reynolds number varying between 1.4×10^6 at the root to 0.75×10^6 at the tip. Measurements from the Delft University wind tunnel at a Reynolds number of 1×10^6 gave a maximum lift coefficient of

1.061, quite close to the value at the 63% section (1.10)

5.1 The ratio of the lift and drag forces

As was the case with the different aspect ratios in figures 6a and 6b the characteristics of the various blade sections differ quite a bit, especially if we look at the deep stall region when leading edge separation is present between 20 and 60 degrees.
For the three sections of figure 8 the lift-drag ratios are displayed in figure 9, together with the two-dimensional characteristic from the CSU wind tunnel

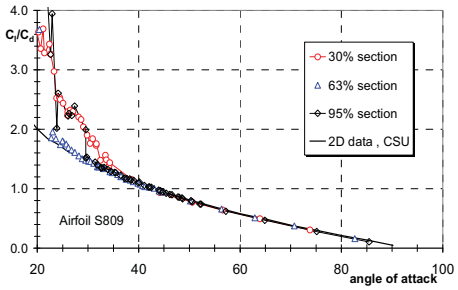

Figure 9: The lift-drag ratio's for 2d and the various blade sections of the NREL phase VI blade.

The figure demonstrates a good agreement between the lift-drag ratio's of the two-dimensional curve and of the various blade stations in the range from 35 degrees to 85 degrees. The same holds for the 47% and 80% span sections, which for clarity reasons have not been plotted in the graph. End effects are noticeable in the onset of leading edge separation for the 30% and 95% blade stations, since their deep-stall angle lies between 30 and 35 degrees compared to the two-dimensional value of 20 degrees.

6 Blade force ratios on a rotating blade.

In [16] Tangler and Kocurek come to the conclusion that the lift-drag ratios of the five different blade sections of the UAE-experiment in the rotating situation closely follow flat plate values. In the light of the fact that the l/d of airfoils in deep stall differ from the flat plate values (figure 5) but that on the other hand the non-rotating values coincide with the two-dimensional curve (figure 9) it seems logic to compare the lift-drag characteristics of the five blade sections in the rotating situation with the values for the two-dimensional airfoil.
Figure 10 gives the lift curves for 4 of the 5 sections of the UAE-H experiment, for which the lift and drag have been derived from the measured pressure distributions with the method described in chapter 5.

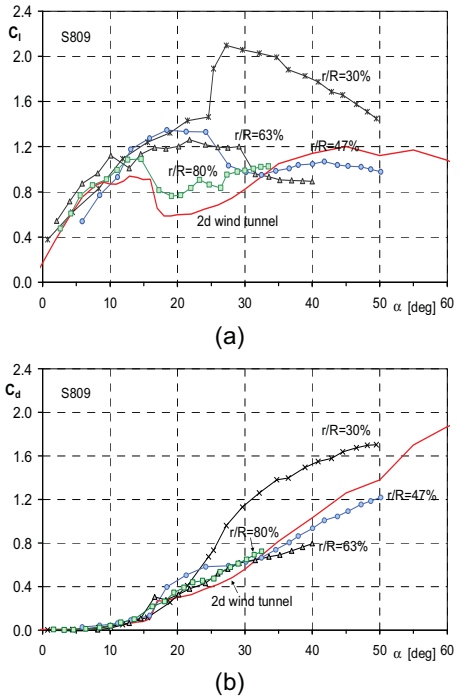

Figure 10: The lift and drag curves for a number of sections of the UAE-rotating blade.

Augmented lift is clearly present in the figure as compared to the two-dimensional curve from the CSU wind tunnel. However, also the drag for the 30% section is significantly higher relative to the two-dimensional case.
Figure 11 shows the lift-drag ratios for the section of figure 10. The graph demonstrates that the lift-drag ratio of the rotating sections eventually all coincide with the two-dimensional curve. The 30% section is projected to touch the 2d curve at about 55 degrees, while the other three sections all fall on this curve at 35 degrees. It appears that when the airfoil is in deep stall, i.e. the boundary layer separates from the leading edge, it makes no difference if the blade rotates or not, the ratio of the lift and drag forces will be the same since they originate from the

pressure distribution dominated by the suction surface pressure

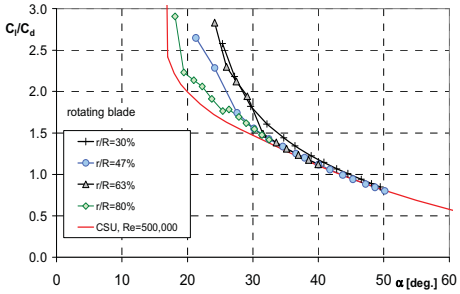

Figure 11: The lift-drag ratios of 4 sections of the UAE rotating blade compared to the 2d wind tunnel curve.

7 Conclusion

A number of experimental airfoil characteristics at high angles of attack found in literature have been studied, with a focus on the maximum drag coefficient and the lift-drag ratio. Furthermore the effect of aspect ratio and a rotating and non-rotating blade on the lift-drag ratio of the blade airfoil has been presented. From the study the following conclusions can be drawn:

- The relation between the maximum drag coefficient and the y/c ordinate of the upwind airfoil contour at x/c=0.0125 can be approximated by a straight line:

  $C_{d,max}=1.994-5.4375*y/c$

- The lift-drag ratios for a number of airfoils with a moderate lower surface thickness coincide at deep stall angles

- The measured lift-drag ratios of an airfoil in deep stall is independent of aspect ratio.

- The lift-drag ratios of the various sections of the non-rotating and rotating NREL UAE phase VI blade in deep stall coincide with the 2d experimental curve.

References

[1] C.C. Critzos, H.H. Heyson, R.W. Boswinkle Jr. "Aerodynamic characteristics of NACA 0012 airfoil at angles of attack from 0 to 180 degrees". NACA TN 3361, 1955

[2] P. Poisson-Quinton, A. de Sievers. "Etude aerodynamique d'un élément de pale d'hélicoptère". Agard Conference Proceedings No. 22, Fluid Dynamics of rotor and fan supported aircraft at subsonic speeds, pp. 4.1 - 4.35, September 1967.

[3] G. Massini, E. Rossi, S. D'Angelo. "Wind tunnel measurements of aerodynamic coefficients of asymmetrical airfoil sections for wind turbine blades extended to high angles of attack". EC DG-XII Contract number: EN3W - 0018 - I, Conclusive Rapport. ENEA - Comitato Nazionale per la Ricerca e per lo Sviluppo dell'Energia Nucleare e delle Energie Alternative, Roma.

[4] R.E. Sheldahl, P.C. Klimas. "Aerodynamic Characteristics of Seven Symmetrical Airfoil Sections Through 180-Degree Angle of Attack for Use in Aerodynamic Analysis of Vertical Axis Wind Turbines. Report SAND80-2114, Sandia Laboratories, Albuquerque, March 1981.

[5] A. Michos, G. Bergeles and N. Anthanassiadis, (National Technical University of Athens) "Aerodynamic characteristics of NACA 0012 airfoil in relation to wind generators". *Wind Engineering Vol. 7, No. 4 pp. 247-261*, 1983

[6] D. Satran and M.H. Snyder. "Two-dimensional tests of GA(W)-1 and GA(W)-2 airfoils at angles-of-attack from 0 to 360 degrees". *Wind Energy report no. 1*, Wind Energy Laboratory, Wichita State University, Kansas, USA, January 1977

[7] A.W. Bloy and D.G. Roberts, "Aerodynamic characteristics of the NACA 63_2-215 aerofoil for use in wind turbines", *Wind Engineering Vol. 17, No.2, 1993, pp.67-75*

[8] C. Ostowari, D. Naik, "Post Stall Studies of Untwisted Varying Aspect